


Nearly free phonons in a weak soliton potential and the case of twisted bilayer grapheneBenoit Van Troeye , Michael Lamparski, Natalya Sheremetyeva, and Vincent Meunier *Department of Physics, Applied Physics, and Astronomy, Rensselaer Polytechnic Institute, Troy, New York 12180, USA*

(Received 24 April 2020; revised 14 December 2021; accepted 16 December 2021; published 18 January 2022)

Structural relaxation in slightly misaligned bilayer graphene leads to the formation of domains separated by topological solitons. The influence of such a soliton lattice on phonons is investigated in the framework of the Frenkel-Kontorova model, where a solution is derived in the continuum limit. A nearly free phonon model is developed to explain the characteristic features in the phonon band structure derived from the Frenkel-Kontorova model. Its 2D extension is discussed and applied on the specific case of twisted bilayer graphene. This model explains a number of computational results reported until now and can be used directly to investigate other misaligned two-dimensional networks as found in van der Waals heterostructures.

DOI: [10.1103/PhysRevB.105.035420](https://doi.org/10.1103/PhysRevB.105.035420)**I. INTRODUCTION**

With the recent discovery of unconventional superconductivity and strongly correlated physics in twisted bilayer graphene (tBLG) [1,2], this system has become a platform of choice to observe exotic phenomena in 2D materials [3–5]. Recent theoretical works have aimed at providing an explanation on the origin of these phenomena, both by considering their electronic [1,5–9] and vibrational [10–15] properties, as well as the coupling between them [11,14,16–19]. In contrast to the aligned bilayer case where the graphene layers are stacked rigidly on top of each other, the in-plane relaxation of tBLG is significant, especially for small twist angles [6,8,9,11,14,20–26] and are related to the formation of a superlattice, the so-called moiré pattern. The influence of this relaxation on the electronic and vibrational properties has already been highlighted previously [1,5–9,12,27]. This relaxation can be interpreted as the formation of domains. Some domains are favored energetically. They correspond to the AB and BA stacking arrangements and they become predominant for small twist angles. In contrast, other domains are disfavored and thus minimized. They correspond to the AA stacking arrangement. The AB and BA domains are separated from each other by domain walls or, in other words, topological solitons, since they are energetically equivalent.

Solitons can be encountered in a broad variety of nonlinear problems in physics, including, nonexhaustively, the Sine-Gordon, Korteweg–de Vries, or nonlinear Schrödinger equations [28,29]. Accordingly, they are of particular relevance in the Frenkel-Kontorova (FK) model [29,30], which consists of a 1D chain of atoms placed onto a periodic potential with a different periodicity. In this case, one possible ground-state configuration corresponds to the periodic repetition of solitons, referred to in the following as the soliton lattice, which modulates the chain lattice in a nonlinear fashion and separates domains where the atoms of the chain are in close registry with the minima of the external potential [30]. Within this approximation, interactions between solitons and other quasiparticles of the system, such as phonons, can

be investigated. Notably, previous theoretical and numerical investigations have highlighted the emergence of band gaps in the phonon band structure at specific wave vectors [29,31–35] as well as the appearance of an optical phonon branch [33–35], but have mostly focused on an incommensurate soliton lattice or a specific solution. Similar features have been observed numerically in the phonon band structure of tBLG [12,27] but also experimentally [36], with the appearance of spatially localized phonon side-bands close to the G peak in the nano-Raman hyperspectral imaging.

In this paper, we examine theoretically how phonons are affected, in general, by the formation of the periodic soliton network, first in the FK model (Sec. II) and, second, in tBLG (Sec. IV). For the former, our results are consistent with previous theoretical and numerical reports on the incommensurate soliton network, and additional features are highlighted in the periodic case analyzed here. Notably, the position and magnitude of the band gap openings are entirely characterized as a function of the parameters of the problem. Then, we rationalize the results obtained in the FK model with the introduction of the nearly free phonon (NFP) model, which is the phonon counterpart of the nearly free electron (NFE) model [37]. The differences between these two models are highlighted. Next, the case of tBLG is discussed as well as how it is related to the NFP model. We discuss how, by geometrical construction of the problem, the phonon band structure is no longer characterized by band-gap openings but instead by the emergence of subbands. This model provides a theoretical account for recent numerical [12,27] and experimental [36] findings.

II. PHONONS IN PERIODIC SOLITON NETWORK (1D FK MODEL)

The mathematical derivations that will be presented hereafter rely essentially on the FK model [29,30,38,39], whose extended solution can be found in the literature [30]. This model consists of a 1D chain of atoms placed onto a periodic potential of different periodicity. For notation, the (initial)

interatomic distance in the chain is denoted a_0 , its spring constant is λ , the amplitude of the external potential is \tilde{V}_0 , and its period is b . The chain consists of $2N + 1$ atoms, each labeled by an index n and positioned at the x_n coordinate along the x axis. The total energy of this system can be written as (for a finite-size system):

$$E = \sum_{n=-N}^{N-1} \frac{\lambda}{2} (x_n - x_{n-1} - a_0)^2 - \sum_{n=-N}^N \tilde{V}_0 \cos\left(\frac{2\pi}{b} x_n\right). \quad (1)$$

The force experienced by the n th atom is

$$F_n = -\lambda(2x_n - x_{n-1} - x_{n+1}) - \tilde{V}_0 \frac{2\pi}{b} \sin\left(\frac{2\pi}{b} x_n\right), \quad (2)$$

which must vanish at equilibrium for each atom of the chain. The problem can be solved analytically in the continuum limit [30], i.e., considering that the atoms continuously accommodate the external potential as a function of the index n . The influence of the lattice discreteness on the static and dynamical solutions of the FK problem are discussed in detail in Ref. [38]. In the context of the continuum limit [30], it is more convenient to work with the phase factor φ_n ,

$$x_n = nb + \frac{b}{2\pi} \varphi_n, \quad (3)$$

which varies continuously and thus implies that $2x_n - x_{n-1} - x_{n+1} \approx -(b/2\pi) \partial^2 \varphi_n / \partial n^2$. It can be shown then that the (general) solution of Eq. (2) is

$$\sin\left(\frac{\varphi}{2} + \frac{\pi}{2}\right) = \text{sn}\left(\frac{\beta n}{k}, k^2\right), \quad (4)$$

where $\text{sn}(n, k^2)$ is the Jacobi elliptic sine function [40,41]. For eccentricity k with $\beta = (2\pi/b)(\tilde{V}_0/\lambda)^{1/2}$. In the description of elliptic integrals, k is also called the elliptic modulus and k^2 the elliptic parameter. In the present case, it is also an integration constant of the problem. For the sake of clarity, the second argument of the Jacobi elliptic function will be omitted in the following, i.e., $\text{sn}(n) \triangleq \text{sn}(n, k^2)$.

Equation (4) corresponds to a periodic array of solitons (kinks), in which the chain is either in compression or in expansion depending on its mismatch with the potential period [38]. Away from these solitons, the atoms of the chain tend to fall into the bottom of the external potential. The solitons are spaced periodically from each other with a periodicity

$$P = \frac{2k}{\beta} K(k^2), \quad (5)$$

where $K(k^2)$ is the complete elliptic integral of the first kind [40], whose argument was already encountered in Eq. (4). If the chain ends are free, the value of k is determined by [30]

$$\frac{E(k^2)}{k} = \frac{\pi}{4} \sqrt{\frac{\lambda}{\tilde{V}_0}} |b - a_0| \triangleq \frac{\pi}{2\sqrt{2}} \sqrt{\frac{\Delta E_{\text{elast}}}{-E_{\text{coher}}}}, \quad (6)$$

where $E(k^2)$ is the complete elliptic integral of the second kind [40] and where we have defined

$$\Delta E_{\text{elast}} = \frac{k}{2} (b - a_0)^2, \quad (7)$$

the elastic cost to exactly match the chain with the potential period, and

$$E_{\text{coher}} = -\tilde{V}_0, \quad (8)$$

which is known as the coherency energy, resulting from the accommodation of the chain with the external potential. Note that the solution discussed hitherto in Eq. (4) is only valid provided [30]

$$\tilde{V}_0 < \gamma_{\text{FK}} \frac{\lambda}{2} (b - a_0)^2, \quad (9)$$

with $\gamma_{\text{FK}} = \pi^2/8$. Indeed, when the external potential amplitude overcomes this threshold, the solution of the problem is a coherent interface, i.e., a structure where the atoms of the 1D chain are in exact registry with the potential minima ($x_n = nb$).

We now turn to the dynamics of the system. The equation of motion for atom n is

$$m \frac{\partial^2 x_n}{\partial t^2} = -\lambda(2x_n - x_{n-1} - x_{n+1}) - \tilde{V}_0 \frac{2\pi}{b} \sin\left(\frac{2\pi}{b} x_n\right), \quad (10)$$

where m is the mass of the atoms constituting the chain (we assume that each atom has an identical mass). In the continuum limit, this equation is the Sine-Gordon equation [38], whose solutions can be obtained using the inverse scattering method [42] and consist of the asymptotic superposition of phonons, solitons, and breathers. Since the Sine-Gordon equation is exactly integrable [38], all these quasiparticles interact elastically with one another. Phonons are already solutions of the equation of motion for the isolated chain, while solitons and breathers directly arise from the nonlinear character of the differential equation. Solitons have already been encountered in the static solution of the FK problem [see Eq. (4)] and are related to localized compression/expansion of the lattice. Breathers correspond to nonlinear periodic oscillations localized in space [38], in contrast with phonons, which are delocalized. Both solitons and breathers are relativistic particles, i.e., their speed cannot overcome the speed of sound in the medium.

In this paper, we focus exclusively on phonons. To the best of our knowledge, they have generally been studied without considering the underlying soliton network accompanying the atomic relaxation of the chain, except for the works of Sutherland [32] and of McMillan [31] where a particular solution was found. We hereafter derive a more general solution. In the case of a coherent interface, the dispersion relation can be easily derived, as done, e.g., in Ref. [38],

$$m\omega^2 = 4\lambda \sin^2 \frac{q}{2} + \tilde{V}_0 \left(\frac{2\pi}{b}\right)^2, \quad (11)$$

where ω is the phonon frequency and q the phonon wave number. Compared to an isolated 1D chain, the only effect of the external potential is thus to transform an acoustic mode into an optical one. This expresses the fact that, when the chain is translated rigidly, there is now an increase of total energy since the atoms are moved away from the bottom of the external potential. This translates into a resistance to sliding, i.e., a nonzero phonon ($\omega \neq 0$) at the zone center ($q = 0$).

More generally, we are interested in the dispersion relation for the semicoherent interface, i.e., the one where the formation of a superlattice is observed. We investigate here the solution far from the chain ends, i.e., within the periodic array of solitons. To investigate the corresponding phonon dispersion, we introduce the time-dependent atomic displacement with respect to the equilibrium position $u_n(t)$,

$$x_n(t) = x_n^0 + u_n(t), \quad (12)$$

where x_n^0 is the static solution of the FK problem, as determined by Eq. (4) following the continuum approach of Frank and Van der Merwe [30]. The equation of motion becomes

$$\begin{aligned} m \frac{\partial^2 u_n}{\partial t^2} = & -\lambda(2u_n - u_{n-1} - u_{n+1}) + \frac{\lambda b}{2\pi} \frac{\partial^2 \varphi_n^0}{\partial n^2} \\ & - \tilde{V}_0 \frac{2\pi}{b} \left[\sin \varphi_n^0 \cos \left(\frac{2\pi}{b} u_n \right) \right. \\ & \left. + \cos \varphi_n^0 \sin \left(\frac{2\pi}{b} u_n \right) \right]. \end{aligned} \quad (13)$$

Considering sufficiently small atomic displacements ($u_n \ll b$), the sine and cosine functions of these atomic displacements can be linearized around the origin. In addition, note that

$$\frac{\lambda b}{2\pi} \frac{\partial^2 \varphi_n^0}{\partial n^2} - \tilde{V}_0 \frac{2\pi}{b} \sin \varphi_n^0 = 0 \quad (14)$$

since at equilibrium, the force on each atom vanishes. With these considerations, equation of motion Eq. (13) becomes

$$m \frac{\partial^2 u_n}{\partial t^2} = -\lambda(2u_n - u_{n-1} - u_{n+1}) - \tilde{V}_0 \left(\frac{2\pi}{b} \right)^2 \cos \varphi_n^0 u_n. \quad (15)$$

One can directly see that $u_n = \bar{u}_n(\omega) \exp(-j\omega t)$ is an acceptable solution of this equation. Thus,

$$m\omega^2 \bar{u}_n = \lambda(2\bar{u}_n - \bar{u}_{n-1} - \bar{u}_{n+1}) + \tilde{V}_0 \left(\frac{2\pi}{b} \right)^2 \cos \varphi_n^0 \bar{u}_n. \quad (16)$$

The dispersion relationship is not as straightforward as the one obtained for the coherent interface, since $\cos \varphi_n^0$ depends explicitly on n , i.e.,

$$\cos \varphi_n^0 = 2 \sin^2 \left(\frac{\varphi_n^0}{2} + \frac{\pi}{2} \right) - 1 = 2 \sin^2 \left(\frac{\beta n}{k} \right) - 1. \quad (17)$$

Inserting the last expression into Eq. (16) leads to the discrete counterpart of the Lamé differential equation [43]. While the solutions of this particular problem can be expressed at the continuum limit in terms of ellipsoidal harmonics [32,43], we present hereafter another approach that relies on perturbation theory [44]. This approach greatly simplifies the analytical expressions.

We first note that Eq. (17) is periodic, and thus can be expanded as a Fourier series (α_t Fourier coefficients). Since it is directly related to Jacobi elliptical functions, it can also

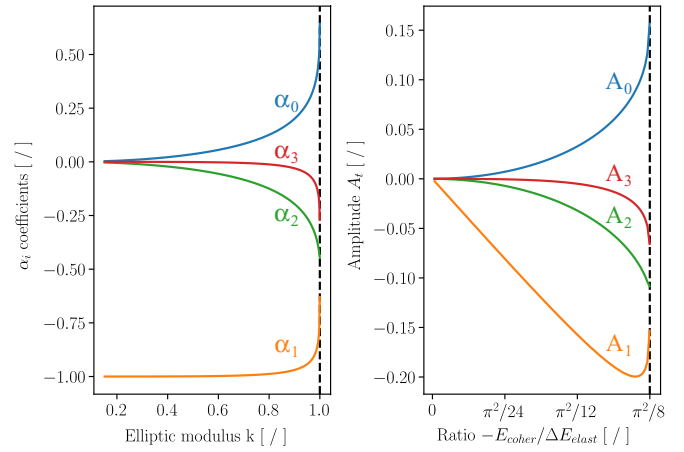


FIG. 1. Left: Variation of the four first Fourier coefficients α_t of the external potential $\cos(\varphi_n^0)$ as a function of the elliptic modulus k . Note that the functions have been truncated to $k \in [0, 0.99989]$ for sake of clarity; all of them, except α_0 , go asymptotically to 0 when $k \rightarrow 1$. Right: Variation of the corresponding amplitude A_t [see Eq. (21)] as a function of the ratio between coherency and elastic energies [see Eqs. (7) and (8)]. The lattice mismatch has been fixed to 10% for illustration. The dashed vertical line corresponds to the asymptotic value for the semicoherent interface. Beyond this line, the coherent interface [whose phonon dispersions are given by Eq. (11)] becomes energetically favored.

be written as a Lambert series [41],

$$\begin{aligned} \cos \varphi_n^0 = & \sum_{t=0}^{\infty} \alpha_t \cos(tQn) = 2 \frac{K(k^2) - E(k^2)}{k^2 K(k^2)} - 1 \\ & - \frac{4\pi^2}{k^2 [K(k^2)]^2} \sum_{t=1}^{\infty} \frac{t \xi^t}{1 - \xi^{2t}} \cos(tQn), \end{aligned} \quad (18)$$

where $E(k)$ is the complete elliptic integral of the second kind and where we have introduced the nome of k ,

$$\xi = \exp \left(\frac{-\pi K(1 - k^2)}{K(k^2)} \right), \quad (19)$$

and Q , the characteristic wave number of the system, i.e.,

$$Q = \frac{2\pi}{P} = \frac{\beta\pi}{kK(k^2)}. \quad (20)$$

The variation of the top four coefficients of the Fourier decomposition in Eq. (17) as a function of k is shown in Fig. 1. As one can see, the Lambert series converges rapidly when k is sufficiently small. It is only at the extreme vicinity of $k \rightarrow 1$ that a high number of harmonics of Q has to be considered. In this case, this Fourier decomposition may not be the most suitable approach to solve the problem. A better option may be to expand the Jacobi sine function in terms of hyperbolic functions instead (see Ref. [40] for further details). This aspect will not be discussed further here.

It is also important to note that, although $\alpha_1 \rightarrow -1$ when $k \rightarrow 0$, this asymptotic value does not correspond to the minimal amplitude of the corresponding harmonic in Eq. (16). Indeed, the integration constant k is determined by Eq. (6) and is a function of the amplitude potential, which is also involved in Eq. (16). Introducing the speed of sound in the medium

$v_s^2 = k/m$ and the lattice mismatch $\Delta = (b - a_0)/b$ between the chain and the potential, Eq. (16) can be written as

$$\omega^2 \bar{u}_n = v_s^2 \left(2\bar{u}_n - \bar{u}_{n-1} - \bar{u}_{n+1} + \sum_t \alpha_t \frac{-E_{\text{coher}}}{\Delta E_{\text{elast}}} 2\pi^2 \Delta^2 \cos(tQn) \bar{u}_n \right) = v_s^2 \left(2\bar{u}_n - \bar{u}_{n-1} - \bar{u}_{n+1} + \sum_t A_t \cos(tQn) \bar{u}_n \right), \quad (21)$$

where $A_t \triangleq 2\pi^2 \Delta^2 \alpha_t (-E_{\text{coher}}/\Delta E_{\text{elast}})$. The variation of the amplitude A_t of the top four components of the Fourier decomposition as a function of the ratio between coherency and elastic energy are shown in the right panel of Fig. 1. As one can see, A_1 varies approximately linearly with respect to the energy ratio, except in the vicinity of $\pi^2/8$, where it reaches a minimal value. Note that all amplitudes except A_0 go to 0 when $-E_{\text{coher}}/\Delta E_{\text{elast}} \rightarrow \pi^2/8$. Their decreasing part is not represented in Fig. 1 for clarity.

Next, we can truncate Eq. (18) to keep only the static term (α_0 coefficient) and the first harmonic of Q frequency (α_1 coefficient). In this case, the differential equation to be solved is

$$m\omega^2 \bar{u}_n = \lambda(2\bar{u}_n - \bar{u}_{n-1} - \bar{u}_{n+1}) + \tilde{V}_0 \left(\frac{2\pi}{b} \right)^2 \alpha_0 \bar{u}_n + \tilde{V}_0 \left(\frac{2\pi}{b} \right)^2 \alpha_1 \cos(Qn) \bar{u}_n, \quad (22)$$

which could be interpreted as the discrete counterpart to Mathieu's differential equation [40]. To solve this problem, we rely on perturbation theory [44] where the external potential term is treated as a perturbation to the system. It is thus assumed that the external potential term is small compared to the elastic term. We rewrite Eq. (22) as

$$\epsilon \bar{u}_n = \hat{\Lambda} \bar{u}_n + \gamma \hat{V} \bar{u}_n, \quad (23)$$

where we have introduced $\epsilon = m\omega^2$ and γ the dimensionless perturbation parameter. The operator $\hat{\Lambda}$ is defined as

$$\hat{\Lambda} \bar{u}_n \triangleq \lambda(2\bar{u}_n - \bar{u}_{n-1} - \bar{u}_{n+1}), \quad (24)$$

while the operator \hat{V} is defined as

$$\hat{V} \bar{u}_n \triangleq \tilde{V}_0 \left(\frac{2\pi}{b} \right)^2 \alpha_0 \bar{u}_n + \tilde{V}_0 \left(\frac{2\pi}{b} \right)^2 \alpha_1 \cos(Qn) \bar{u}_n. \quad (25)$$

The eigenvalues are expanded in terms of γ ,

$$\epsilon = \epsilon^{(0)} + \gamma \epsilon^{(1)} + \gamma^2 \epsilon^{(2)} + \dots, \quad (26)$$

and similarly for the eigenvectors

$$\bar{u}_n = \bar{u}_n^{(0)} + \gamma \bar{u}_n^{(1)} + \gamma^2 \bar{u}_n^{(2)} + \dots \quad (27)$$

The unperturbed solution is $\epsilon^{(0)} = 4\lambda \sin^2 q$ associated with the eigenvector $\bar{u}_n^{(0)} = (P)^{-1/2} e^{\pm jqn}$, where P is the period of the superlattice as defined by Eq. (5). The first-order correction to the energy is

$$\epsilon^{(1)} = \langle \bar{u}_n^{(0)} | \hat{V} | \bar{u}_n^{(0)} \rangle = \tilde{V}_0 \left(\frac{2\pi}{b} \right)^2 \alpha_0, \quad (28)$$

since the average of $\cos(Qn)$ over the period P is zero. Using first-order perturbation theory, the effect of the external potential is a rigid translation in ω^2 , and thus corresponds to the transformation of an acoustic phonon into an optical phonon

(see Fig. 2). This is observed for any value of the integration constant k , although the shift reduces to 0 for $k \rightarrow 0$. This effect is exactly the same as the one described for a coherent interface [see Eq. (11)], still in a weaker form: The atoms are not all situated at the bottom of the external potential in the case of a semicoherent interface. The resistance to sliding of this system is thus smaller, since it is *averaged* over all the atomic sites in the superlattice. In parallel, if there is no accommodation of the external potential, i.e., the atomic sites equally cover the positions corresponding to positive and negative values of the external potential, translating the chain does not modify the energy of the system since it falls back to an equivalent energy configuration (translational invariance).

The analysis so far indicates that only the static term is involved in the first-order perturbation theory. However, the first overtone of the external potential will be involved in the second order and beyond. This requires a careful treatment of the energy degeneracy between the different eigenvectors of the unperturbed case. In the unperturbed solution, there are two phonon branches, corresponding to positive and negative wave vectors. A linear combination of these solutions is

$$\bar{u}_n = \frac{1}{\sqrt{P}} (c_+ e^{jqn} + c_- e^{-jqn}), \quad (29)$$

where c_+ and c_- are the coefficients of the linear combination. One finds

$$\begin{aligned} & \langle \bar{u}_n | \hat{\Lambda} | \bar{u}_n \rangle \\ &= \frac{1}{P} (c_+^* \quad c_-^*) \begin{pmatrix} 4\lambda \sin^2(q/2) & 0 \\ 0 & 4\lambda \sin^2(q/2) \end{pmatrix} \begin{pmatrix} c_+ \\ c_- \end{pmatrix} \end{aligned} \quad (30)$$

and

$$\begin{aligned} \langle \bar{u}_n | \hat{V} | \bar{u}_n \rangle &= \tilde{V}_0 \left(\frac{2\pi}{b} \right)^2 \frac{1}{P} (c_+^* \quad c_-^*) \\ & \begin{pmatrix} \alpha_0 & \frac{\alpha_1}{2} (\delta_{2q,-Q} + \delta_{2q,Q}) \\ \frac{\alpha_1}{2} (\delta_{2q,-Q} + \delta_{2q,Q}) & \alpha_0 \end{pmatrix} \begin{pmatrix} c_+ \\ c_- \end{pmatrix}, \end{aligned} \quad (31)$$

where δ_{ij} denotes the Kronecker delta. To derive these expressions, the orthogonality between the e^{jqn} and e^{-jqn} functions has been used. The effects of the α_0 terms correspond to the first-order perturbation theory described above. Thus, one can directly see that, at second order, the external potential only affects two points, i.e., $Q/2$ and $-Q/2$. At $Q/2$, the degeneracy between $\omega_{Q/2}^2$ and $\omega_{-Q/2}^2$ states is lifted, leading to the two following phonon states:

$$m\omega_{\pm}^2(Q/2) = 4\lambda \sin^2 \left(\frac{Q}{4} \right) + \tilde{V}_0 \left(\frac{2\pi}{b} \right)^2 \alpha_0 \pm \tilde{V}_0 \left(\frac{2\pi}{b} \right)^2 \frac{\alpha_1}{2}. \quad (32)$$

By convention, ω_- is defined as the lowest energy state at $q = Q/2$, while ω_+ is the highest one. The eigenvectors associated

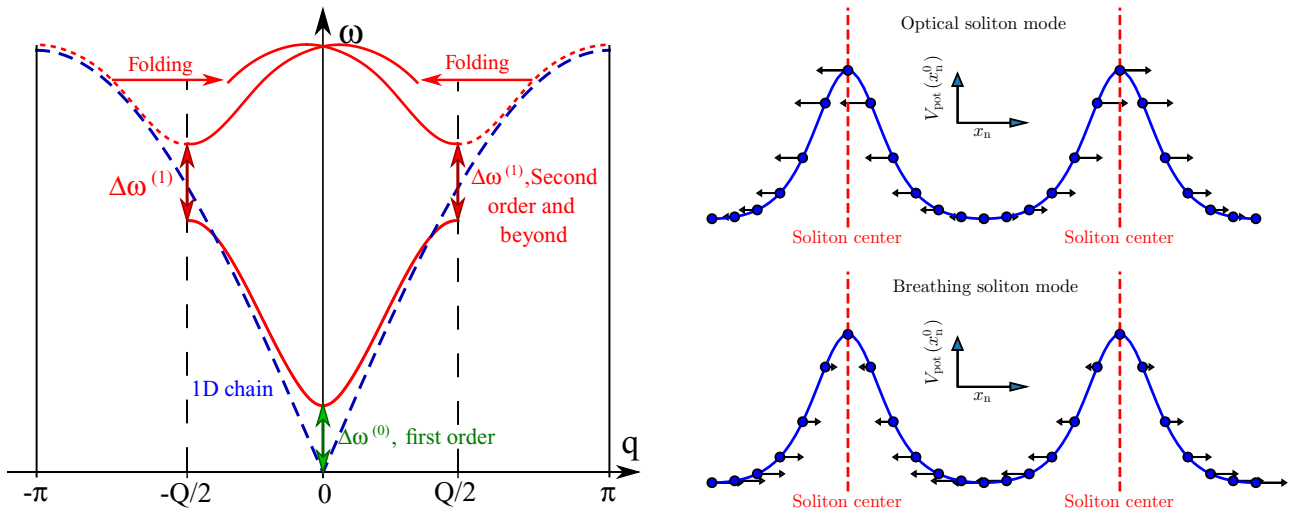


FIG. 2. Left: Schematic representation of the influence of the external potential on the phonon band structure of a 1D chain of atoms. The unperturbed case is depicted in dash blue while the perturbed case is shown in red. The soliton potential transforms the acoustic mode into an optical mode ($\Delta\omega^{(0)}$ frequency shift at $q = 0$) and opens band gaps in the phonon band structure at $q = \pm Q/2$ (solid red: $\Delta\omega^{(1)}$ opening; only the first harmonic is represented for clarity). Since the system is periodic, one can equivalently only consider the superlattice's Brillouin zone. The states outside of this zone are then folded inside the superlattice's Brillouin zone (dotted red onto solid red). Right: Schematic representation of the phonon states at the band-gap opening, where each circle represents an atom of the chain. The y axis corresponds to the external potential energy for a given atom and is only represented for clarity. Arrows represent the norm of the phonon eigenvector. The modes at the band-gap opening can either be interpreted as an optical soliton vibration (upper mode) or as a breathing soliton vibration (lower mode).

with these phonon states are

$$\bar{u}_n^-(Q/2) = \frac{1}{\sqrt{2P}}(e^{jQn/2} + e^{-jQn/2}) = \frac{2}{\sqrt{2P}} \cos(Qn/2) \quad (33)$$

and

$$\bar{u}_n^+(Q/2) = \frac{1}{\sqrt{2P}}(e^{jQn/2} - e^{-jQn/2}) = \frac{2j}{\sqrt{2P}} \sin(Qn/2), \quad (34)$$

and correspond to stationary waves, which are either localized around the soliton core [Eq. (33)] or, on the contrary, away in the coherent domains [Eq. (34)]. The phonon states at $-Q/2$ are associated with the same frequencies as the ones at $Q/2$, but their eigenvectors are complex conjugates of Eqs. (33) and (34). They are schematically represented in Fig. 2 and could be interpreted as optical soliton [Eq. (33)] and breathing soliton [Eq. (34)] excitations, respectively.

The effect of the first potential harmonic is represented graphically in Fig. 2 and corresponds to a band-gap opening at the $Q/2$ and $-Q/2$ points. This adds to the already discussed effect of the static term (transformation of an acoustic mode into an optical mode). Note that, referring to Fig. 1, the band-gap opening varies approximately linearly over a large portion of the function domain, reaching a maximum in absolute value when the ratio between the coherency and elastic energies lies in the close vicinity of $\pi^2/8$.

It can easily be shown that the effect of the higher harmonics of the external potential [Eq. (18)] is almost identical to the one derived for its first harmonic, i.e., the opening of band gaps at the $tQ/2$ wave numbers, where t is the index of the corresponding t th harmonics and $t \in \mathbb{Z}_0$, the ensemble of nonzero integers. Let us now consider the soliton lattice, associated with its own Brillouin zone, i.e., $[-Q/2, Q/2]$, which

contains all the information on phonons and is a fraction of the 1D chain's Brillouin zone. Compared to the 1D chain's case, the details coming from wave numbers away from this superlattice Brillouin zone are simply *folded* on the irreducible Brillouin zone (see Fig. 2 for a graphical sketch). The *even* harmonics fold onto the zero wave number, thus opening a band gap at the zone center, while the *odd* harmonics open a band gap at the zone borders, i.e., $Q/2$ and $-Q/2$.

III. NEARLY FREE PHONON MODEL

This folded representation is reminiscent of the one derived for electrons in the NFE model [37], where the effect of the nucleus potential is to open forbidden band gaps at the zone boundaries and at the zone center. This suggests the introduction of the NFP model, for which the FK model provides analytical results. Two major differences between NFE and NFP models have to be discussed. The first one comes from the fact that the first-order perturbation term, arising from the static term in the Fourier decomposition, is crucial for phonons since it leads to transformation of the acoustic mode into an optical mode, instead of a simple energy shift. Meanwhile, in the NFE model, this static term can be discarded since it simply corresponds to a rigid shift in energy. The second major difference arises from the fact that the dispersion relation is unbound in the NFE model, while it is bound for phonons. The band-gap openings thus happen in a relatively narrow frequency window in contrast with the NFE model. This latter point will be critical when we come back to the slightly misaligned graphene bilayer case.

Following the derivation presented in this section, one can see that the external potential has strong implications for the dispersion relation of a 1D chain. Numerical investigations

of phonons in the FK model [34,35] considering an incommensurate phase (i.e., nonuniformly spaced solitons) have already demonstrated the emergence of an optical branch and of discontinuities in the phonon band structure at nonspecific phonon wave vectors. While some traces of the acoustic model remain in this incommensurate case, our investigations reveal that this feature disappears for a periodically repeated soliton network, as well as that the band-gap openings appear specifically at the superlattice Brillouin zone and at the zone center. As mentioned previously, a specific solution for phonons in the Sine-Gordon equation has also been derived analytically in previous works [31,32]. This specific solution corresponds exactly to the $k \rightarrow 0$ case derived in this paper for the free-end chain configuration (see Fig. 1), where no band gap openings are predicted in the phonon band structure. More general cases always lead to the transformation of the acoustic mode into the optical mode.

IV. PHONONS IN TWISTED GRAPHENE BILAYER

We will now apply our findings to the specific case of tBLG phonons. The following (geometrical) approach shares many similarities with the studies presented in Refs. [6,13,14]. The problem will be approximated as a strictly two-dimensional one. The graphene lattice before relaxation is characterized by the lattice vectors $\mathbf{a}_1 = (0, 1)a$ and $\mathbf{a}_2 = (-\sqrt{3}/2, -1/2)a$, where a is the lattice parameter of graphene. The corresponding reciprocal lattice vectors are $\mathbf{a}_1^* = 2\pi/a(-\sqrt{3}/3, 1)$ and $\mathbf{a}_2^* = 2\pi/a(-2\sqrt{3}/3, 0)$. The position of a given unit cell is $\mathbf{R}_{kl} = k\mathbf{a}_1 + l\mathbf{a}_2$. The atomic positions in the unit cell are $\mathbf{r}_1 = \mathbf{0}$ and $\mathbf{r}_2 = \mathbf{a}_1/3 + 2\mathbf{a}_2/3$. The corresponding atomic index is denoted κ . Furthermore, to distinguish between the two layers, the superscripts B and T are introduced to refer to the bottom and top layers, respectively. For sufficiently small atomic displacements with respect to the equilibrium positions (i.e., in the harmonic approximation), the elastic energy of the system is given by

$$E_{\text{elast}} = \sum_{\kappa\alpha, kl} \sum_{\kappa'\beta, k'l'} \Lambda_{\kappa\alpha, \kappa'\beta}(\mathbf{R}_{kl}, \mathbf{R}_{k'l'}) u_{\kappa\alpha}(\mathbf{R}_{kl}) u_{\kappa'\beta}(\mathbf{R}_{k'l'}), \quad (35)$$

where $\Lambda_{\kappa\alpha, \kappa'\beta}(\mathbf{R}_{kl}, \mathbf{R}_{k'l'})$ are the interatomic force constants between the atoms situated at $\mathbf{r}_\kappa + \mathbf{R}_{kl}$ and at $\mathbf{r}_{\kappa'} + \mathbf{R}_{k'l'}$ coordinates in the directions α and β , while $u_{\kappa\alpha}(\mathbf{R}_{kl})$ expresses the displacement along the direction α of the atom κ in the cell (k, l) with respect to its equilibrium position. The force experienced by the atoms when one of them is moved away from its equilibrium position varies thus linearly in this harmonic approximation.

Next, the bottom graphene layer is rotated by an angle $\theta/2$ clockwise, while the top layer is rotated by an angle $\theta/2$ counterclockwise. The position of a graphene unit cell in the bottom layer is thus given by

$$\mathbf{R}_{kl}^B = \underline{\underline{\Omega}}_{-\theta/2} \mathbf{R}_{kl} = \begin{pmatrix} \cos(\theta/2) & \sin(\theta/2) \\ -\sin(\theta/2) & \cos(\theta/2) \end{pmatrix} \mathbf{R}_{kl}, \quad (36)$$

while the position of a graphene unit cell in the top layer is given by $\mathbf{R}_{kl}^T = \underline{\underline{\Omega}}_{\theta/2} \mathbf{R}_{kl}$. The interatomic force constants are

also transformed after rotation:

$$\underline{\underline{\Lambda}}_{\kappa, \kappa'}^B(\mathbf{R}_{kl}, \mathbf{R}_{k'l'}) = \underline{\underline{\Omega}}_{\theta/2} \underline{\underline{\Lambda}}_{\kappa, \kappa'}(\mathbf{R}_{kl}, \mathbf{R}_{k'l'}) \underline{\underline{\Omega}}_{-\theta/2} \quad (37)$$

and

$$\underline{\underline{\Lambda}}_{\kappa, \kappa'}^T(\mathbf{R}_{kl}, \mathbf{R}_{k'l'}) = \underline{\underline{\Omega}}_{-\theta/2} \underline{\underline{\Lambda}}_{\kappa, \kappa'}(\mathbf{R}_{kl}, \mathbf{R}_{k'l'}) \underline{\underline{\Omega}}_{\theta/2}. \quad (38)$$

Without any lattice relaxation, the relative position of a cell in the bottom layer with respect to the corresponding cell in the top layer is given by

$$\begin{aligned} \delta_{kl} &= \mathbf{R}_{kl}^B - \mathbf{R}_{kl}^T \\ &= 2a \sin(\theta/2) [(1, 0)k + (-1/2, \sqrt{3}/2)l]. \end{aligned} \quad (39)$$

For certain values of θ , it is possible to find values of k, l that fulfill $\|\delta_{kl}\| = a$. In those cases, a superlattice can be constructed based on the lattice vectors

$$\mathbf{L}_1 = \frac{a}{2 \sin(\theta/2)} (1, 0) \quad (40)$$

and

$$\mathbf{L}_2 = \frac{a}{2 \sin(\theta/2)} (-1/2, \sqrt{3}/2). \quad (41)$$

In this superlattice, some regions of space can be assimilated to AA and AB stacking; between those areas, the stacking arrangement evolves linearly in the absence of relaxation. The corresponding reciprocal lattice vectors

$$\mathbf{L}_1^* = \frac{4\pi}{a} \sin(\theta/2) (1, \sqrt{3}/3) \quad (42)$$

and

$$\mathbf{L}_2^* = \frac{4\pi}{a} \sin(\theta/2) (0, 2\sqrt{3}/3) \quad (43)$$

form a hexagonal Brillouin zone, whose high-symmetry points are $\mathbf{K}^L = (1/3, 1/3, 0)$ and $\mathbf{M}^L = (1/2, 0, 0)$ in reduced coordinates, respectively. By construction, these points correspond exactly to the difference in positions between the corresponding \mathbf{K} and \mathbf{M} high-symmetry points in the bottom and top layers (see Fig. 3). It means that, in the absence of any interlayer interaction, the phonon states at the \mathbf{K}^L and \mathbf{M}^L include the folded graphene phonon states at the \mathbf{K} and \mathbf{M} high-symmetry points upon a rotation of their phonon eigendisplacements.

The influence of the interlayer interaction is now considered. In the classical picture, it can be written as a summation over pairwise terms,

$$E_{\text{inter}} = \sum_{\kappa, kl} \sum_{\kappa', k'l'} V(\mathbf{r}_{\kappa, k, l}^B - \mathbf{r}_{\kappa', k', l'}^T), \quad (44)$$

where $V(\mathbf{r}_{\kappa, k, l}^B - \mathbf{r}_{\kappa', k', l'}^T)$ is a monotonously decreasing function of the distance between the atoms. Let us suppose that this interlayer energy depends only on the (local) stacking arrangement between the graphene sheets, determined by Eq. (39), independently of the strain state in the layers. In this case, the interlayer energy potential can simply be obtained by spanning the translational energy landscape between the layers in the Bernal bilayer graphene configuration as has been done previously in the literature (see, e.g., Ref. [6]). The

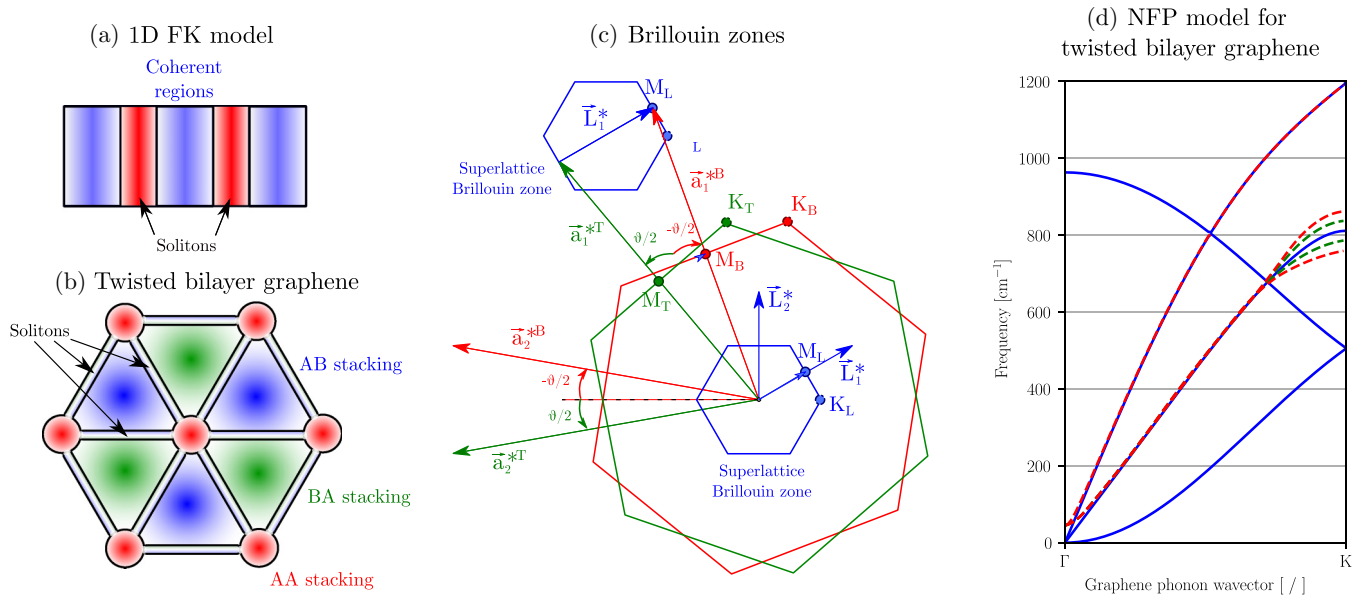


FIG. 3. (a), (b) Schematic representations of the relaxed structures of (a) 1D FK model and (b) twisted bilayer graphene. Both show domainlike solutions: In the FK model, coherent regions, where the atoms are in close registry with the external potential (in blue) are separated by the other ones by solitons, where the atoms span the other part of the external potential (in red); meanwhile, in twisted bilayer graphene (b), regions of optimal stacking arrangement are favored (in blue and green) and separated from the other by domain walls (solitons). (c) The Brillouin zones of the superlattice (L superscript), and of the top (T superscript) and bottom (B superscript) layers. Right: Schematic application of the NFP model on the graphene bilayer case (initial phonon states in solid blue). Only the first four graphene modes are represented and the $\Gamma \rightarrow K$ branch, and we only illustrate the effect of the NFP model on the transverse acoustic mode here. The modes with in-plane character are affected by the soliton potential, leading to band-gap openings at the K high-symmetry point (first harmonic of the potential in dashed red, third in dashed green). Note the appearance of an optical mode at low frequency.

interlayer energy can be written in terms of a Fourier series

$$E_{\text{inter}} = \sum_{kl} \sum_{nm} \tilde{V}_{nm} \exp(j\mathbf{G}_{nm}^L \cdot \delta_{kl}), \quad (45)$$

where \tilde{V}_{nm} are the Fourier coefficients and \mathbf{G}_{nm}^L are linear combinations of the superlattice reciprocal lattice vectors, i.e., $\mathbf{G}_{nm}^L = n\mathbf{L}_1^* + m\mathbf{L}_2^*$. The interlayer energy is minimum for the AB stacking arrangement and maximum for the AA stacking one. During relaxation, the system preferentially adopts these AB stacking regions and tends to minimize the AA stacking ones by further misaligning the layers locally around these regions, as has already been shown several times in the literature [6,11,14,20–24].

With this approximated interlayer potential, the problem strongly resembles the FK model that has been described previously, except that the problem is now 2D and the relevant input parameters, i.e., elastic and external potentials, take more complicated forms. Solving this extended problem goes beyond the scope of this paper; nevertheless, the relaxation observed in practice, both experimentally and computationally, can still be interpreted as the formation of a soliton network in the system [see Fig. 3(b)] [6,11,14,20–24]. The NFP model described in the previous section can be applied on slightly misaligned bilayer graphene and gives some insight into the phonon band structure of the twisted system. Some subtleties emerge in the specific case of twisted bilayers, which will now be discussed.

The NFP model indicates that one can expect band-gap openings in the phonon band structure at the high-symmetry

points of the superlattice Brillouin zones, i.e., at Γ^L , \mathbf{K}^L , and \mathbf{M}^L . In the simple FK picture, the amplitude of these band-gap openings would be directly proportional to the coefficients of the Fourier decomposition given by Eq. (45), with $V_{nm} \rightarrow 0$ for $\mathbf{G}_{nm}^L \rightarrow \infty$. Still, not all the graphene modes are expected to be affected by this soliton network potential. First, if the corrugation (i.e., out-of-plane displacements) is neglected, only the phonons with in-plane character will be perturbed. This does not mean that the out-of-plane phonons should not be impacted by the interlayer potential—of course, a layer breathing mode emerges when the graphene layers are stacked on top of the others independently of the formation of a superlattice [45]—but the NFP model is unable to describe them. This aspect also comes into play when a phonon mode shares both in-plane and out-of-plane characters. For the sake of simplicity, we suppose here that a mode corresponds to atomic motions that are entirely in plane or out-of-plane. Second, there is translational invariance: a rigid shift of the system does not modify its energy. In a simple perturbation picture, the translational mode in bilayer graphene arising from the combination of the in-plane translational modes in phase should not be affected by the soliton network formation since the potential depends on the relative positions between the atoms [see Eqs. (44) and (45)]. In contrast, the combination of modes in opposite phases are affected, leading to the appearance of an optical mode in the phonon spectrum. This is confirmed by a brute force computational approach [27].

At this stage, one expects the emergence of phonon band gaps at the high-symmetry points of the superlattice's

Brillouin zone. By geometrical construction, these high-symmetry points are directly related to their corresponding high-symmetry points in the Brillouin zone of the graphene bottom and top layers [see Fig. 3(c)]. This means that the band-gap openings affect the phonon modes at these high-symmetry points, i.e., the (in-plane) graphene phonon modes at Γ , M , and K of the graphene Brillouin zone. We focus here specifically on the high-symmetry line between the Γ and K points [see Fig. 3(d)] and on the effect of the soliton potential on the K point [46]. Its first harmonic along that direction is expected to open a band gap for phonons with in-plane character at the K , as represented schematically in red in Fig. 3(d). We now consider the third harmonic of the soliton potential in that direction, which falls on the K point of a further graphene Brillouin zone. Since the dispersion relationship of phonons is bound, this higher harmonic acts on the very same initial phonon mode for the band gap opening, i.e., the phonon mode of graphene at the K high-symmetry point [see Fig. 3(d) in dashed green]. This result contrasts with the 1D FK model presented in Sec. II, where—in general—the higher harmonics of the potential were affecting different phonon modes.

This feature, specific to slightly misaligned bilayers (i.e., not only to tBLG), has important consequences: Not only one harmonic of the soliton potential, but an infinity, are acting on the same initial phonon states at the high-symmetry points of the layer Brillouin zones (see Fig. 3). This explains the observation of numerous subbands at the high-symmetry points of the unfolded Brillouin zone in our previous numerical investigation of the tBLGs phonon band structures [12,27]. From the 1D FK model, they should be associated to eigendisplacements localized around the domain walls, or on the contrary

in the coherent domains. The effect of harmonics with really large wave vectors are expected to be negligible except when $k \rightarrow 1$. A similar trend can be observed numerically in tBLG for a small misalignment angle $\theta \rightarrow 0^\circ$ [27]. Experimentally, Raman peaks, specifically localized in space either in the soliton core or in the AA region, have been recently reported [36]. Once again, they can be understood based on this NFP model.

V. CONCLUSION

We have theoretically examined how the presence of a periodic soliton lattice affects the phonons, as encountered in the 1D FK model and in tBLG systems. The former case can be solved analytically in the continuum limit and using perturbation theory, and the solutions suggest the introduction of the NFP model. For tBLG, we use this NFP model to explain the emergence of phonons subbands at the high-symmetry points of the unfolded graphene Brillouin zone. While we have focused exclusively on tBLG systems, the emergence of numerous subbands in the phonon band structure is also expected in other twisted bilayers like MoS₂-MoS₂ and other transition-metal dichalcogenide bilayers.

ACKNOWLEDGMENTS

This work is supported by the NY State Empire State Development's Division of Science, Technology and Innovation (NYSTAR) through Focus Center-NY-RPI Contract No. C150117. N.S. was supported by NSF Grant No. EFRI 2-DARE (EFRI-1542707).

-
- [1] Y. Cao, V. Fatemi, S. Fang, K. Watanabe, T. Taniguchi, E. Kaxiras, and P. Jarillo-Herrero, *Nature (London)* **556**, 43 (2018).
 - [2] Y. Cao, V. Fatemi, A. Demir, S. Fang, S. L. Tomarken, J. Y. Luo, J. D. Sanchez-Yamagishi, K. Watanabe, T. Taniguchi, E. Kaxiras *et al.*, *Nature (London)* **556**, 80 (2018).
 - [3] M. Yankowitz, S. Chen, H. Polshyn, Y. Zhang, K. Watanabe, T. Taniguchi, D. Graf, A. F. Young, and C. R. Dean, *Science* **363**, 1059 (2019).
 - [4] A. L. Sharpe, E. J. Fox, A. W. Barnard, J. Finney, K. Watanabe, T. Taniguchi, M. A. Kastner, and D. Goldhaber-Gordon, *Science* **365**, 605 (2019).
 - [5] E. Codecido, Q. Wang, R. Koester, S. Che, H. Tian, R. Lv, S. Tran, K. Watanabe, T. Taniguchi, F. Zhang *et al.*, *Sci. Adv.* **5**, eaaw9770 (2019).
 - [6] N. N. T. Nam and M. Koshino, *Phys. Rev. B* **96**, 075311 (2017).
 - [7] K. Uchida, S. Furuya, J.-I. Iwata, and A. Oshiyama, *Phys. Rev. B* **90**, 155451 (2014).
 - [8] F. Guinea and N. R. Walet, *Phys. Rev. B* **99**, 205134 (2019).
 - [9] P. Lucignano, D. Alfè, V. Cataudella, D. Ninno, and G. Cantele, *Phys. Rev. B* **99**, 195419 (2019).
 - [10] A. I. Cocemasov, D. L. Nika, and A. A. Balandin, *Phys. Rev. B* **88**, 035428 (2013).
 - [11] Y. W. Choi and H. J. Choi, *Phys. Rev. B* **98**, 241412(R) (2018).
 - [12] M. Angeli, E. Tosatti, and M. Fabrizio, *Phys. Rev. X* **9**, 041010 (2019).
 - [13] M. Koshino and Y.-W. Son, *Phys. Rev. B* **100**, 075416 (2019).
 - [14] M. Koshino and N. N. T. Nam, *Phys. Rev. B* **101**, 195425 (2020).
 - [15] H. Ochoa, *Phys. Rev. B* **100**, 155426 (2019).
 - [16] T. J. Peltonen, R. Ojajärvi, and T. T. Heikkilä, *Phys. Rev. B* **98**, 220504(R) (2018).
 - [17] F. Wu, A. H. MacDonald, and I. Martin, *Phys. Rev. Lett.* **121**, 257001 (2018).
 - [18] G. S. N. Eliel, M. V. O. Moutinho, A. C. Gadelha, A. Righi, L. C. Campos, H. B. Ribeiro, P.-W. Chiu, K. Watanabe, T. Taniguchi, P. Puech *et al.*, *Nat. Commun.* **9**, 1221 (2018).
 - [19] B. Lian, Z. Wang, and B. A. Bernevig, *Phys. Rev. Lett.* **122**, 257002 (2019).
 - [20] J. S. Alden, A. W. Tsun, P. Y. Huang, R. Hovden, L. Brown, J. Park, D. A. Muller, and P. L. McEuen, *Proc. Natl. Acad. Sci.* **110**, 11256 (2013).
 - [21] M. M. van Wijk, A. Schuring, M. I. Katsnelson, and A. Fasolino, *2D Mater.* **2**, 034010 (2015).
 - [22] S. Dai, Y. Xiang, and D. J. Srolovitz, *Nano Lett.* **16**, 5923 (2016).

- [23] S. K. Jain, V. Juričić, and G. T. Barkema, *2D Mater.* **4**, 015018 (2016).
- [24] H. Yoo, R. Engelke, S. Carr, S. Fang, K. Zhang, P. Cazeaux, S. H. Sung, R. Hovden, A. W. Tsen, T. Taniguchi *et al.*, *Nat. Mater.* **18**, 448 (2019).
- [25] F. Gargiulo and O. V. Yazyev, *2D Mater.* **5**, 015019 (2017).
- [26] M. Angeli, D. Mandelli, A. Valli, A. Amaricci, M. Capone, E. Tosatti, and M. Fabrizio, *Phys. Rev. B* **98**, 235137 (2018).
- [27] M. Lamparski, B. V. Troeye, and V. Meunier, *2D Mater.* **7**, 025050 (2020).
- [28] N. J. Zabusky and M. D. Kruskal, *Phys. Rev. Lett.* **15**, 240 (1965).
- [29] O. Braun, Y. Kivshar, and Y. Kivshar, *The Frenkel-Kontorova Model: Concepts, Methods, and Applications*, Physics and Astronomy Online Library (Springer-Verlag, Berlin, 2004).
- [30] F. C. Frank and J. H. van der Merwe, *Proc. R. Soc. London* **198**, 205 (1949).
- [31] W. L. McMillan, *Phys. Rev. B* **16**, 4655 (1977).
- [32] B. Sutherland, *Phys. Rev. A* **8**, 2514 (1973).
- [33] A. D. Novaco, *Phys. Rev. B* **22**, 1645 (1980).
- [34] S. Aubry, *J. Phys. France* **44**, 147 (1983).
- [35] M. Peyrard and S. Aubry, *J. Phys. C: Solid State Phys.* **16**, 1593 (1983).
- [36] A. C. Gadelha, D. A. A. Ohlberg, C. Rabelo, E. G. S. Neto, T. L. Vasconcelos, J. L. Campos, J. S. Lemos, V. Ornelas, D. Miranda, R. Nadas *et al.*, *Nature (London)* **590**, 405 (2021).
- [37] K. M. Rabe, *Phys. Today* **55**(12), 61 (2002).
- [38] O. M. Braun and Y. S. Kivshar, *Phys. Rep.* **306**, 1 (1998).
- [39] P. Bak, *Rep. Prog. Phys.* **45**, 587 (1982).
- [40] M. Abramowitz and I. A. Stegun, *Handbook of Mathematical Functions with Formulas, Graphs, and Mathematical Tables* (Dover, New York, 1964).
- [41] S. C. Milne, *Ramanujan J.* **6**, 7 (2002).
- [42] M. J. Ablowitz, D. J. Kaup, A. C. Newell, and H. Segur, *Phys. Rev. Lett.* **30**, 1262 (1973).
- [43] E. T. Whittaker and G. N. Watson, *A Course of Modern Analysis*, 4th ed., Cambridge Mathematical Library (Cambridge University Press, Cambridge, 1996).
- [44] C. Cohen-Tannoudji, B. Diu, and F. Laloë, *Mécanique quantique II* (Hermann, Paris, 1972).
- [45] Note that the frequency of the corresponding mode can vary with the size of the superlattice and the degree of lattice reconstruction.
- [46] We have also represented the zone center contribution responsible for the appearance of the optical mode at Γ .